Korean J. Chem. Eng., 40(7), 1746-1759 (2023)
DOI: 10.1007/s11814-023-1439-6

pISSN: 0256-1115
eISSN: 1975-7220

Effect of spinning parameter on the properties and performance of hollow fiber supported liquid membrane for levulinic acid extraction

Vikneswary Rajendaren, Syed Mohd Saufi†, and Mior Ahmad Khushairi Mohd Zahari

Faculty of Chemical and Process Engineering Technology, Universiti Malaysia Pahang, Lebuhraya Tun Razak, 26300 Gambang, Pahang Darul Makmur, Malaysia

(*Received 19 September 2022 • Revised 7 January 2023 • Accepted 31 January 2023*)

Abstract−A hollow fiber-supported liquid membrane (HFSLM) configuration with a large membrane surface area per volume is becoming more viable and feasible to use on an industrial scale. However, the hollow fiber (HF) forms a thicker skin outer layer than its flat-sheet equivalents, resulting in lower membrane fluxes and more unsatisfactory performance. Therefore, this study investigated the effect of HF spinning parameters such as bore liquid type, air gap distance (3-12 cm), and air relative humidity (64-100 wt%) on the properties and performance of HFSLM for levulinic acid (LA) extraction. The HF membranes were characterized in terms of morphology, contact angle, porosity, and membrane tensile strength. Polyethersulfone-based HF membrane prepared using 60% v/v dimethylacetamide as bore liquid at 6 cm air gap distance and 86% air relative humidity resulted in the highest LA extraction of 72.2%. The membrane had a dual symmetric finger-like structure with an open porous structure. The value of the outer fiber surface contact angle, porosity, and tensile stress was 94.1°, 77.57%, and 1,524.7 kPa, respectively. An optimal spinning condition is crucial in producing the best HF structure for improving the HFSLM performance in LA extraction.

Keywords: Hollow Fiber, Levulinic Acid, Spinning Parameter, Supported Liquid Membrane

INTRODUCTION

Levulinic acid (LA) is one of the top biorefinery products for the chemical industry that is being planned and developed worldwide [1]. However, the most significant issue to consider in developing a cost-effective and efficient LA production technology is the separation or recovery of LA during the process. Generally, the downstream processing accounts for about 50% to 70% of the LA overall production cost [2]. The current methods available for LA separation are expensive, inefficient, and have poor environmental consequences [3]. In our recent studies, supported liquid membranes (SLM) showed great potential for LA recovery from the aqueous solution [4,5]. The SLM process provides a maximum driving force for separating the desired solute, thus leading to high removal rates. In addition, SLM is more efficient than liquid-liquid extraction [6].

Practically, the flat sheet-supported liquid membrane (FSSLM) was investigated during the development stage to test the feasibility of using SLM to extract the targeted component. However, due to the small surface area-to-volume ratio of the FSSLM, it is not attractive to implement at industrial scale [7]. Therefore, hollow fiber (HF) membrane configuration with a large membrane surface area per volume is becoming more viable and feasible to use on the industrial scale [8]. Compared to the flat sheet membrane, the manufacture of the HF membrane is more challenging and requires numerous fabrication parameters that must be regulated. The optimum HF membrane for the SLM procedure should have an ideal skin thickness and good pore structure. It is best to prevent the creation of thick, dense layers since they have a detrimental impact on the performance of extraction and membrane fluxes. A study of the HF manufacturing parameters is therefore essential to develop appropriate HF characteristics and thereby enhance LA extraction by HFSLM.

During HF production, a suitable internal coagulant (known as bore liquid) is required to eliminate the thick skin layer formation in the outer fiber and to improve the pore size of the inner skin layer. A previous study showed that using pure water as bore liquid resulted in instantaneous demixing and formed a dense outer skin layer with tiny pores in the membrane [9]. When a potassium acetate solution was used as the bore, a highly selective skin layer at the inner surface of the polyethersulfone (PES) HF was produced [10]. Alternatively, a mixture of the solvent and pore-forming agent in the bore liquid can reduce the concentration difference between the chemical present in the bore liquid and the dope solution. Consequently, the water can diffuse into the dope solution and grow up the initiated nuclei before the phase separation is fully completed [9]. This prevents the formation of the thick outer skin layer and enhances the pore formation at the inner surface of the fiber.

An air gap distance highly impacts the morphology, pore structure properties, and surface hydrophobicity of the HF membrane [11,12]. An increase in the air gap from 3 cm to 50 cm in the polysulfone (PSF) HF membrane reduced fiber thickness and increased the porosity and average pore size on the outer fiber surface [12]. An increment in the air gap also can reduce the outer and inner diameter of the HF membrane [13]. Moreover, Korminouri et al. [11] reported that increasing the air gap ranging from 1 to 20 cm

†To whom correspondence should be addressed.
E-mail: smsaufi@ump.edu.my

improved the hydrophobicity of the polyvinylidene fluoride (PVDF) membrane surface.

Air gap distance also affects the shape of the HF lumen. It was observed that the lumen of the hybrid PES/polyvinyl alcohol HF membrane, which was fabricated at a low air gap of 5 cm, looked oval. It became a circular shape at a higher air gap distance [13]. Furthermore, the air gap distance affects the pore structure of the membrane. High air gap distance produces a less finger-like void structure of the PES HF membrane [14]. A high air gap causes stretching and elongation of the nascent fiber by their weight during exiting from the spinneret. Thus, the polymer aggregates move closer together and rearrange themselves to a higher degree of stability [14]. Hence, it is vital to manipulate the air gap distance to achieve the desired property of the HF membrane support for SLM.

During the dry-wet spinning process, the dope is initially exposed to humid air before being immersed in a coagulation bath. The non-solvent from the humidified air penetrates the polymer solution and initiates a phase separation. In the presence of water vapor, the solvent/non-solvent exchange rate will be slow [15]. This avoids the quick formation of a skin layer and provides adequate time to form pore nucleation and growth [16]. As a result, a skinless morphology with a relatively large pores membrane is obtained.

A study on the effect of relative humidity (37%, 60%, and 80%) on the flat sheet PVDF membrane morphology, contact angle, and liquid entry pressure was conducted by AlMarzooqi et al. [17]. At low PDVF concentration, the contact angle and pore size increased as relative humidity and vapor exposure time increased [17]. The effects of a hybrid flat sheet PES-graphene membrane fabricated at air humidity ranging from 70% to 100% on removing acetic acid by SLM were studied by Harruddin et al. [18]. Based on the results, the cast film exposed to air humidity at 80% for 30 s and then immersed in a coagulation bath at 50 °C produced the most suitable membrane support for SLM.

To the best of our knowledge, LA separation through HFSLM has never been studied before. It is essential to understand the effect of the spinning parameters on the HF membrane structure to produce the desired membrane structure for LA extraction using HFSLM. Hence, this study investigated the effect of the type of bore liquid, air gap distance, and air relative humidity on the HF properties and its performance in LA separation using HFSLM.

METHODOLOGY

1. Materials

PES (Radel® A, Solvay, USA, CAS #28212-68-2), graphene nanopowder (Low Dimensional Materials Research Centre, University of Malaya, Malaysia), polyethylene glycol 200 (PEG 200, Sigma Aldrich, CAS #25322-68-3), and DMAC (Sigma Aldrich, CAS #127-19-5) were mixed to form a dope solution. PEG 200 and DMAC were also used as bore liquids during HF spinning. Tap water was used as the external coagulant. The liquid membrane in the organic phase was formulated using 2-ethyl-1-hexanol (Sigma Aldrich, CAS #104-76-7), and trioctylamine (TOA, Sigma Aldrich, CAS #1116-76-3). LA (Sigma Aldrich, CAS #123-76-2) and sodium hydroxide (NaOH, Merck, CAS #1310-73-2) are the feed and stripping solutions. Olive oil from Delima Oil Products Sdn. Bhd. was used to conduct the membrane porosity test. The potassium dihydrogen phosphate (KH_2PO_4, RM Chemical, CAS #7778-77-0) was used as the mobile phase in HPLC analysis. Sulphuric acid (H_2SO_4, Acros Chemicals, CAS #7664-93-9) was used to adjust the pH value of the mobile phase for HPLC analysis.

2. PES/Graphene Hollow Fiber Fabrication

Dry-wet spinning process was used to fabricate the HF. The dope solution was first prepared by mixing the following dope components: 15 g PES, 42.5 g PEG, 42.5 g DMAC, and 0.015 g graphene. Nitrogen gas of 0.1 MPa pressure was used to push the dope solution through the annulus spinneret of 1.651 mm outer diameter (OD) and 1.194 mm inner diameter (ID). The extruded fiber passed through a specified air gap under controlled humidity before entering the water coagulation bath at 40 °C. At first, four types of bore liquid were tested: water, 60% v/v DMAC in water, 60% PEG 200 in water, and a mixture of 30% v/v DMAC and 30% v/v PEG 200 in water. Then the distance of the air gap and relative humidity in the air gap region was varied in the range of 3-12 cm and 64-100%, respectively. The air at the air gap region was humidified using the mini humidifier (Deerma) by monitoring the humidity value using RH Digital Humidity Controller (Vakind). The HF produced from the spinning machine was immersed in the water at room temperature for 48 h to remove the residual solvent further. The HF was then dried in the open air for 48 h. The dry-wet spinning condition of the HF membrane produced during this study is summarized in Table 1.

3. Membrane Characterization

3-1. Morphology of Membrane

The membranes were frozen in liquid nitrogen and fractured by using forceps. The prepared samples were coated with platinum. The cross-sectional morphology of the membranes was observed by scanning electron microscope (SEM) ZEISS EVO 50. Image J was used to measure the ID and OD of the fibers from three different membrane locations, and the average value for each dimen-

Table 1. Dry-wet spinning condition

No.	Bore fluid	Air gap distance, cm	Relative humidity, %	Notes
1.	Water, 60% v/v DMAC in water, 60% PEG 200 in water, a mixture of 30% v/v DMAC and 30% v/v PEG 200 in water	6	86	To study effect of bore fluid type.
2.	60% v/v DMAC in water	3-12	86	To study effect of air gap distance.
3.	60% v/v DMAC in water	6	64, 86, 100	To study effect of relative humidity.

sion was computed.

3-2. Contact Angle Measurement

The contact angle of the fiber was determined to evaluate the hydrophobicity of the membrane [5]. At room temperature, a small syringe with a stainless steel needle was used to drop 1 μl of H_2O on the HF membrane surfaces. The contact angle between the membrane surface and the water droplet was measured using an optical contact angle measurement system (CAM 101 optical Contact Angle Meter, KSV Instruments). The average contact angle from three different membrane locations was calculated for each membrane sample.

3-3. Porosity Measurement

The porosity of the membrane was measured using olive oil, as reported by Harruddin et al. [18]. The middle slit of the HF membrane (2 cm length) was dried in a vacuum oven at 80 °C for 24 h to remove the water from the fiber completely. The dried fiber was weighed as W_1. Later, the fiber was soaked in olive oil for 24 h to allow the oil to be fully filled within the pores and empty spaces in the fiber. Filter paper was used to remove the excess olive oil on the wet membrane surface. Later, the wet fiber was weighed and recorded as W_2. The fiber porosity ε (%) was calculated using Eq. (1) [18,19]. The fiber porosity of each sample was measured three times to minimize the experimental errors, and the average value was reported.

$$\text{Porosity, } \varepsilon(\%) = \frac{W_2 - W_1}{\rho V_1} \times 100\% \quad (1)$$

where, ε is the HF porosity (%), W_2 is the weight of the wet fiber (g), W_1 is the weight of the dry fiber (g), V_1 is the fiber volume (cm^3), and ρ is the density of oil (0.8 g/cm^3). The empty space in the membrane support was calculated by dividing the total weight of olive oil impregnated in the 30 cm of the membrane by the density of the olive oil.

3-4. Mechanical Strength

The HF sample was cut with a length of 75 mm and dried in the oven overnight at 80 °C. Then the peak load at a crosshead speed of 5 mm/min was determined using a CT3 Texture Analyzer from Brookfield Engineering (USA). The gauge length was 50 mm [20]. The average tensile strength of three membrane samples was measured to get a reliable value. The tensile stress values were calculated using Eq. (2) [21].

Fig. 1. Hollow fiber module.

$$\sigma = \frac{F}{A} \times \frac{1\ \text{kPa}}{1{,}000\ \text{Pa}} \quad (2)$$

where, σ is tensile stress (kPa), F is peak load (N) and A is the cross-section area of the membrane (m^2), respectively.

4. HFSLM System

The module for assembling the HF was constructed based on the configuration suggested by Li et al. [22] using an ½ inch stainless steel tube with a 30 cm length, as shown in Fig. 1. Five HF membranes were inserted into the stainless steel tube and glued at both ends using Loctite E30CL epoxy resin. The organic LM was circulated for 24 h by pumping the solution through the HF lumen at a flow rate of 2 ml/min [23]. Once the fiber was completely filled, it could be observed that LM overflows to the outer fiber side [24]. Deionized water was used for flushing out the excess LM by flowing into the lumen and outer fibers side for 30 min at a flow rate of 1 ml/min [25].

Masterflex L/S peristaltic pump was used to deliver the feed and stripping solution to the HF module in the HFSLM system, as shown in Fig. 2. The feed phase (10 g/L aqueous LA solution) was pumped into the bore of the HF membrane. Meanwhile, the stripping solution (0.5 M NaOH) was fed at the outside fiber bundle in

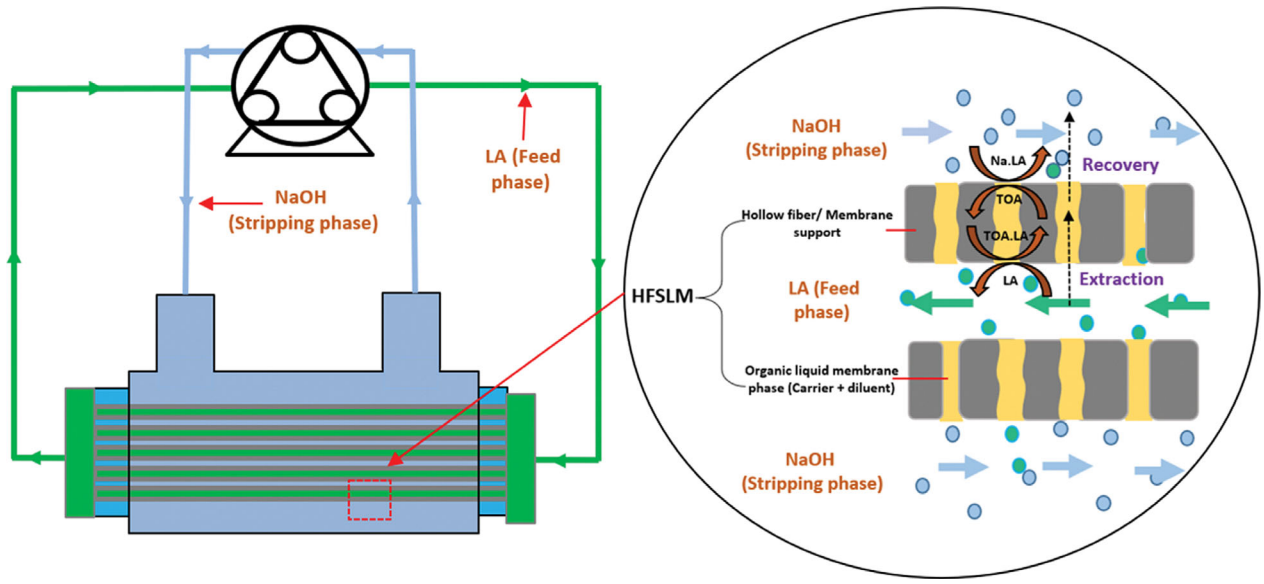

Fig. 2. HFSLM flow configuration.

a counter-current direction [26,27]. The HFSLM was run continuously for 8 h by circulating the feed and stripping solution throughout the HF module.

5. LA Extraction Yield

The concentration of LA in the feed phase was continuously evaluated every 2 h for 8 h HFSLM operation to calculate the LA ex-

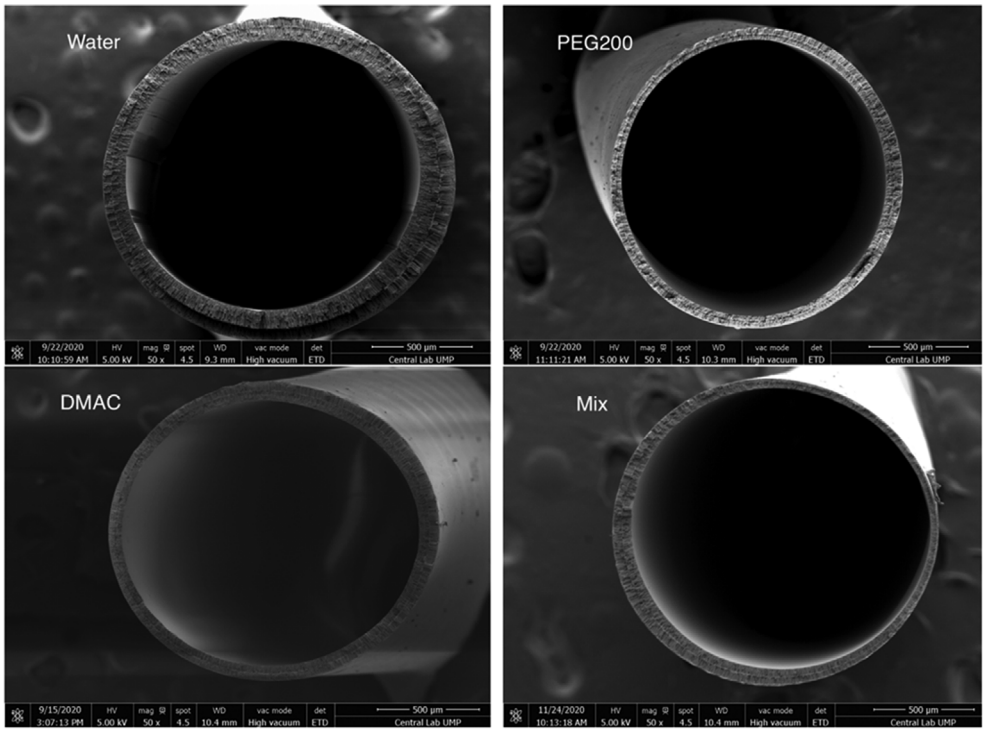

(a)

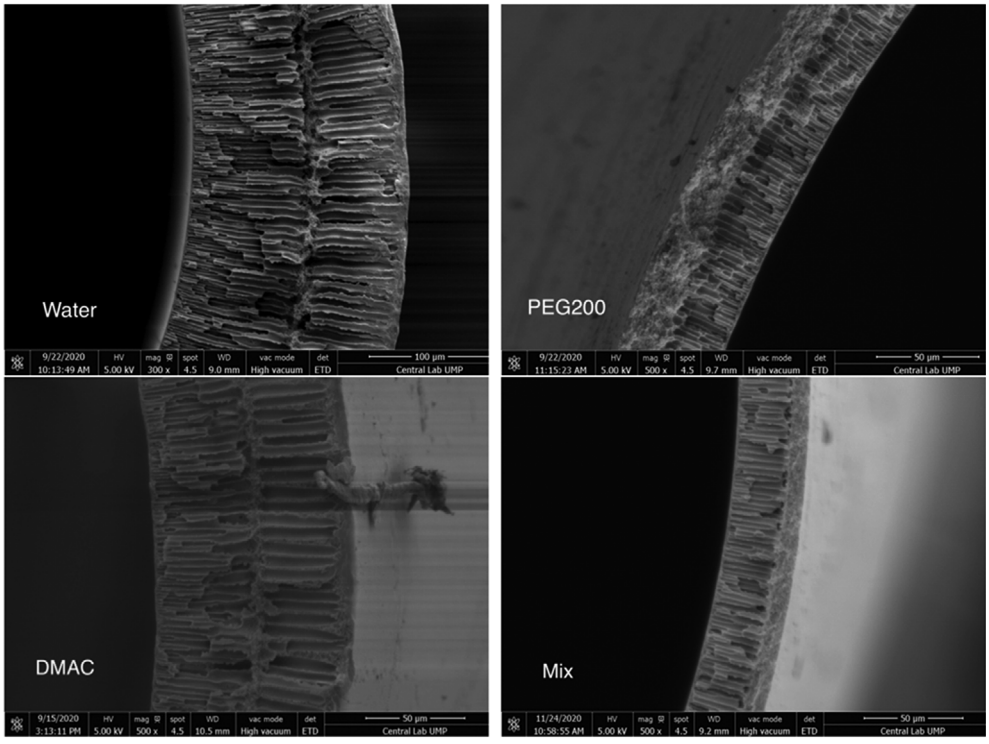

(b)

Fig. 3. Morphology of the HF membrane spun using various types of bore liquids: (a) cross section, (b) thin wall section, (c) thick wall section, (d) outer surface.

traction yield. The concentration of LA in the sample was determined using an Agilent high-performance liquid chromatography (HPLC) 1200 system. Synergy Hydro C18 HPLC column (Phenomenex, 250 mm×4.6 mm, 4 μm particle size) was used in the measurement. The column was operated using 0.02 M potassium dihydrogen phosphate, pH 2.9 as a mobile phase. The peak response was detected using an ultraviolet (UV) detector at 221 nm. A flow rate of 0.8 mL/min was used during the 22-minute operation of the column at 30 °C. Eq. (3) was used to calculate the percentage of LA extracts from the feed phase:

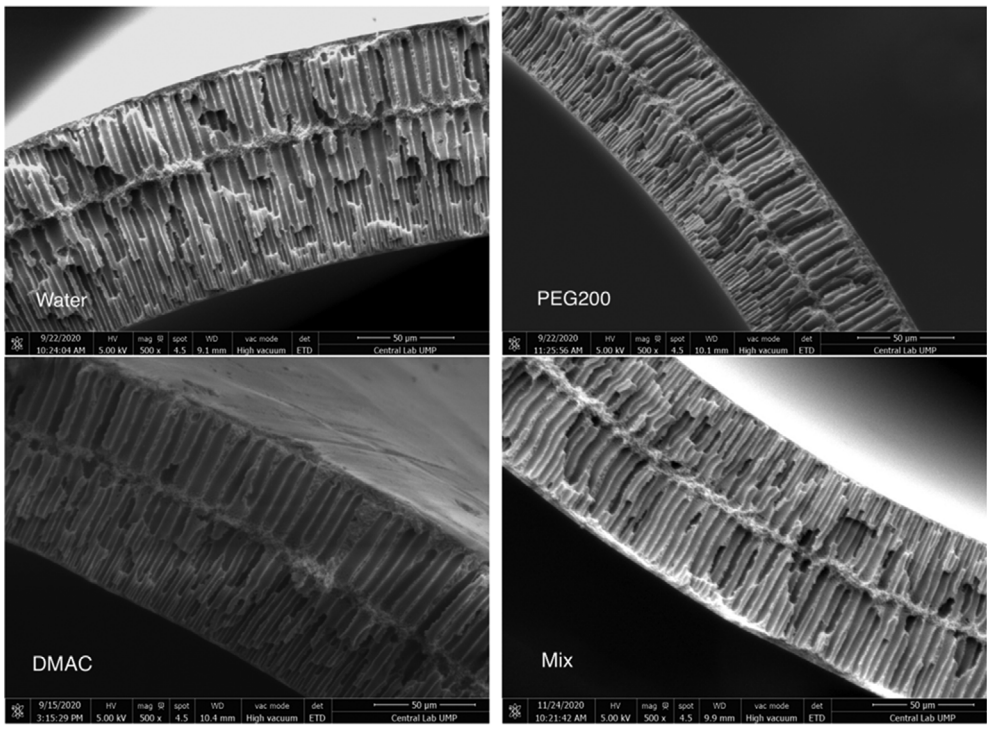

(c)

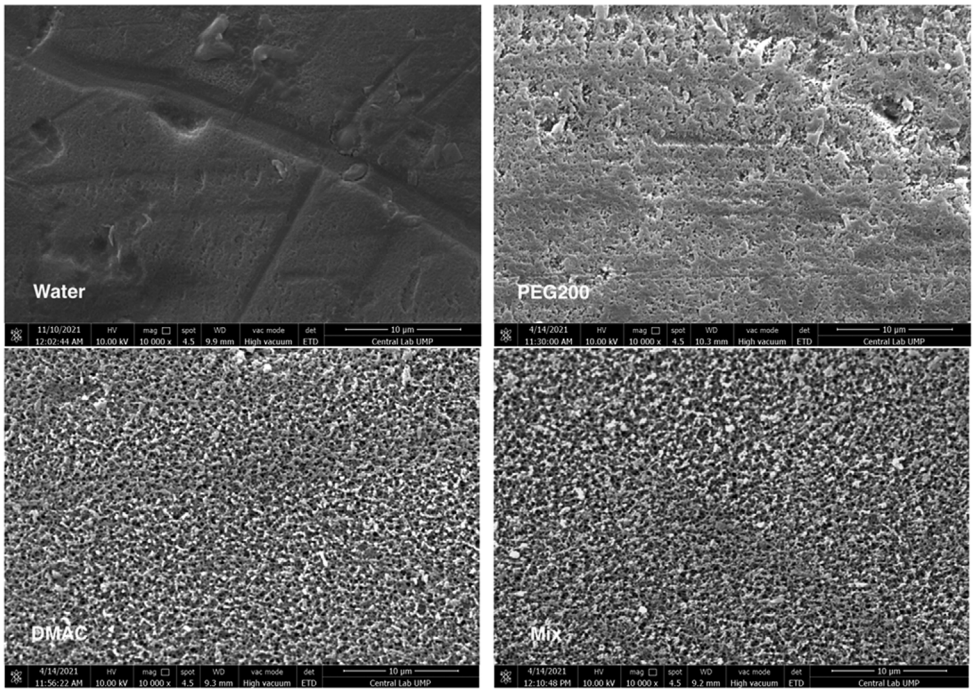

(d)

Fig. 3. Continued.

$$\text{LA extraction (\%)} = \frac{[LA]_{fi} - [LA]_{fo}}{[LA]_{fi}} \times 100\% \quad (3)$$

where $[LA]_{fi}$ and $[LA]_{fo}$ indicate the initial and final LA concentrations in the feed phase, respectively.

RESULTS AND DISCUSSION

1. Effect of Bore Liquid

Water is typically used as the bore liquid during HF membrane fabrication. Water usage as the bore liquid promoted more enormous concentration differences between the DMAC and PEG 200 in the dope solution and bore liquid. Hence, the DMAC can easily and rapidly diffuse from the dope solution into the bore liquid to form a smooth surface inside the HF [9]. However, when the PEG 200 solution, DMAC solution, or mixed solution of PEG 200/DMAC/water was used as the bore liquid, it reduced the concentration difference between the dope solution and bore liquid, thus reducing the diffusion rate of the DMAC and PEG from the dope solution into the bore liquid. Hence the water slowly diffused into the dope solution and initiated the growth of nuclei in the inside skin layer before complete phase separation occurs. According to Fig. 3(a), a dual finger-like symmetric structure in fiber was formed using water and DMAC solution as the bore liquid.

The fibers fabricated using PEG 200 solution and a mixed solution of the bore liquid (i.e., mixture of PEG and DMAC) resulted in the unsymmetric fiber wall structure. The hole inside the fibers was not in the center. Moreover, a thick and thin wall was formed in the fibers. The thick part displayed a dual finger-like structure wall. While the thin layer is made of a dense layer followed by a single finger-like layer, as shown in Fig. 3(b) and 3(c). The water as the bore liquid formed a smooth surface, and the introduction of additive or solvent created a rough surface as similarly reported by Liu et al. [9] and shown in Fig. 3(d).

Table 2 shows the physical properties of the HF fabricated from different types of bore liquids. The contact angle, tensile stress, and LA extraction yield of the HF are shown in Fig. 4, Fig. 5, and Fig. 6, respectively. Water as bore liquid resulted in the thickest fiber wall, 0.1174 mm, with a thick, dense layer at the outer surface. This thick and highly porous fiber comprised a large empty space for oil impregnation. Hence, it had the highest empty space of 0.1463 cm^3 with 88% porosity. Even though it can accommodate the highest amount of LM for LA extraction, the dense outer surface and skin layer at the inside surface interrupt the transportation of the LA from the feed phase to the stripping phase. Therefore, it can only extract the smallest amount of LA from the feed phase, around 11.1% LA. However, the thick, dense, and unsymmetric fiber layer promoted the highest mechanical strength of 2,131.8 kPa. At the same time, the average contact angle reading is 87.7°, as shown in Fig. 4.

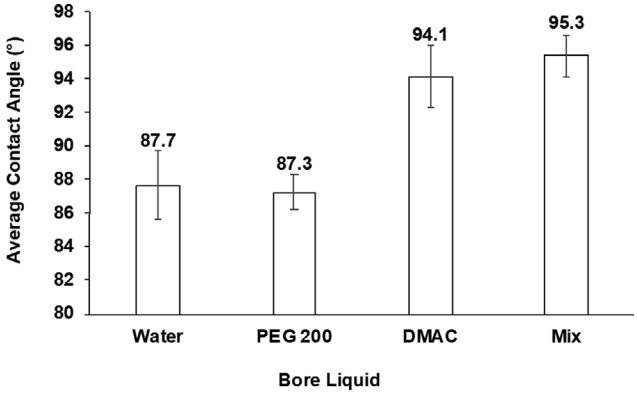

Fig. 4. Contact angle of the HF fabricated using various types of bore liquid.

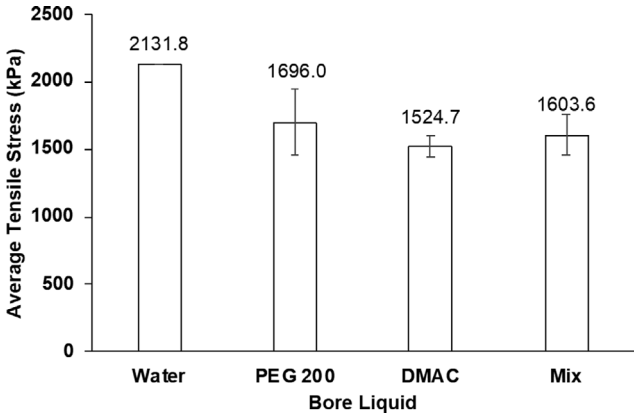

Fig. 5. Tensile stress of the HF fabricated using various types of bore liquid.

The PEG 200 in the bore liquid created a dense layer followed by a finger-like structure with OD 1.5097 mm, ID 1.3734 mm, and a thickness of 0.0682 mm, as shown in Table 2. PEG 200 is a pore-forming agent. Its introduction in the dope solution formed a spongy-like outer surface by preventing finger-like formation, improving pore formation, enhancing pore interconnectivity, and promoting hydrophilicity in the fiber [28]. Therefore, it had the lowest aver-

Table 2. Physical properties of the HF fabricated from different types of bore liquids

Bore Liquid	Water	PEG 200	DMAC	Mix
ID (mm)	1.3840	1.3734	1.3952	1.4420
OD (mm)	1.6187	1.5097	1.5574	1.5837
Wall thickness (mm)	0.1174	0.0682	0.0811	0.0709
Total fiber volume (cm^3)	0.1661	0.0926	0.1128	0.1010
Empty space (cm^3)	0.1463	0.0706	0.0875	0.0750
Porosity (%)	88.07±1.13	76.29±2.34	77.57+2.77	74.24±4.91

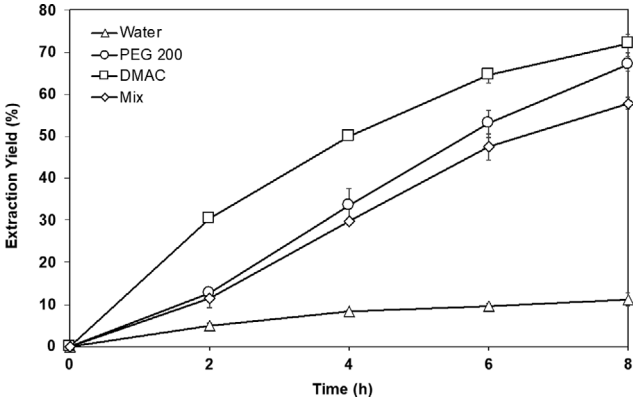

Fig. 6. LA extraction yield of the HF fabricated using various types of bore liquid. Experimental condition: feed phase - 10 g/L LA; stripping phase - 0.5 M NaOH; flow rate - 1 mL/min); LM phase - 0.3 M TOA in 2-ethyl-1-hexanol.

age contact angle of 87.3°. The formation of a dense sponge layer reduced the empty space, 0.0706 cm^3 for the oil impregnation, and drove into low porosity of 76.3%. At the same time, the asymmetric structure of the fiber provided an excellent mechanical strength of 1,696.0 kPa. However, the dense layer restricted the interaction between the stripping and LM organic phases. Consequently, a large amount of LA accumulated in the LM organic phase. The transport of LA-carrier complex was interrupted but still able to give the second highest LA extraction of 67.1%.

Using DMAC as the bore liquid eliminated the formation of a dense layer and formed a porous outer surface of the fiber. It generated two symmetric finger-like structure layers throughout the cross-sectional of the fiber with OD 1.5574 mm, ID 1.3952 mm, and a thickness of 0.0811 mm. The open pores at the outer surface contributed to the high average contact angle of 94.1°. The thick and finger-like macrovoids throughout the fiber improved the porosity of the membrane with a value of 77.6%. At the same time, the symmetric fiber structure led to the lowest tensile stress, around 1,524.7 kPa. The HF prepared from DMAC bore liquid showed the highest LA extraction of 72.2% from the feed phase. The membrane's open structure reduced the LA accumulation in the LM organic phase. The same goes for the fibers from the mixtures of 30% PEG 200, 30% DMAC, and 40% water as bore liquid. It successfully extracted 57.9%. Bang et al. [29] also found that the addition of solvent in the bore liquid improved the ultrafiltration membrane performance. The maximum water flux was obtained when 50% of the solvent was added to the bore liquid, and more than 97% of the bovine serum albumin was rejected.

The morphology of fiber produced from the mixture of 30% PEG 200, 30% DMAC, and 40% water as bore liquid was almost similar to the 60% PEG 200 membrane cross-section structure. It possessed OD 1.5837 mm, ID 1.4420 mm, and a thickness of 0.0709 mm. The introduction of PEG 200 in DMAC solution at bore liquid induced a thin dense layer formation at the outermost surface of the fiber. It is maybe because of the high viscosity of PEG 200, which slowly diffused from the dope solution and formed a smooth and high packing density surface at the outer surface. A porous outer surface was formed when the DMAC was used at bore liquid. The fiber from mixed bore liquid showed the highest contact angle (95.3°) but the lowest porosity (74.2%). The asymmetric fiber had good tensile stress of 1,603 kPa. It successfully extracted 57.9% of LA from the feed phase.

Based on Fig. 6, fibers from DMAC show an efficient extraction of LA at 72.2%. The fiber from mixed bore liquid extracted 57.9% of LA, which is 19.8% lower than the DMAC. Furthermore, the fiber from PEG 200 extracted 13.7% more LA than the mixed bore liquid. Apart from that, the fibers from water indicated the worst performance in the SLM process due to the formation of thick, dense high packing with a non-porous outer surface and skin layer at the inside surface. These surfaces interrupted the transport of the LA from the feed phase to the stripping phase. Thus, it resulted in the least extraction of LA at 11.1%. Therefore, the bore liquid composed of 60% v/v DMAC in water was selected for further study because it successfully created an open porous surface membrane with a high LA extraction of 72.2%.

2. Effect of Air Gap Distance

Fig. 7 shows the morphology of the HF membrane spun at different air gaps. The fibers fabricated at 3 cm and 6 cm air gap consist of dual-layer finger-like structure membranes. The further increased air gap to 9 cm and 12 cm prevented the formation of a finger-like structure and formed a dense layer at the outermost surface of the fibers. The same trend was seen by Khayet [14], who found that extending the PES HF membrane's air gap from 30 cm to 200 cm caused a decrease in the number of finger-like voids. It might be due to the changes in the elongation and shear rates at the outermost point of the outlet of spinnerets [30]. The high external elongation stresses created phase instability and facilitated spinodal decomposition [31]. It induced chain packing at the outermost layer. This chain packing slowed the diffusion of the water into the dope solution while speeding up the radial outflow of spinning solvents from the dope solution [31] Hence, it formed a dense layer [32]. Furthermore, the thickness of the dense layer increased with an increase in the air gap.

Theoretically, the increase in the air gap caused high gravitation pull and high elongation stress on the dope from the spinneret. This dramatically affected the morphology and characteristics of the fabricated fiber [12]. It decreased the inner and outer diameter and the wall thickness of the fiber, as shown in Table 3. It was demonstrated that the OD of the dense and compact outermost layer fiber, which was fabricated at 9 cm, was 14.2% smaller than the dual finger-like structural fiber, which was fabricated at 6 cm. This large shrinkage occurred due to the high elongation stretch on the dope from the spinneret. The shrinkage caused a drastic drop in the thickness of the fiber, around 26%, from an air gap of 6 cm to 9 cm as 0.0811 mm and 0.0600 mm, respectively [31]. Increasing the air gap reduced the fiber thickness and formed a compact, dense structure at the outmost layer of the fiber. These reduced the space available for oil impregnation; therefore, the porosity was reduced over the increase in the air gap.

Fig. 8 and Fig. 9 show the contact angle and tensile stress of the HF prepared at different air gaps. The surface contact angle of the fiber increased when the air gap distance increased. The fiber made from the longest air gap of 12 cm resulted in the highest surface contact angle reading around 100.2°, 24.5% greater than the short-

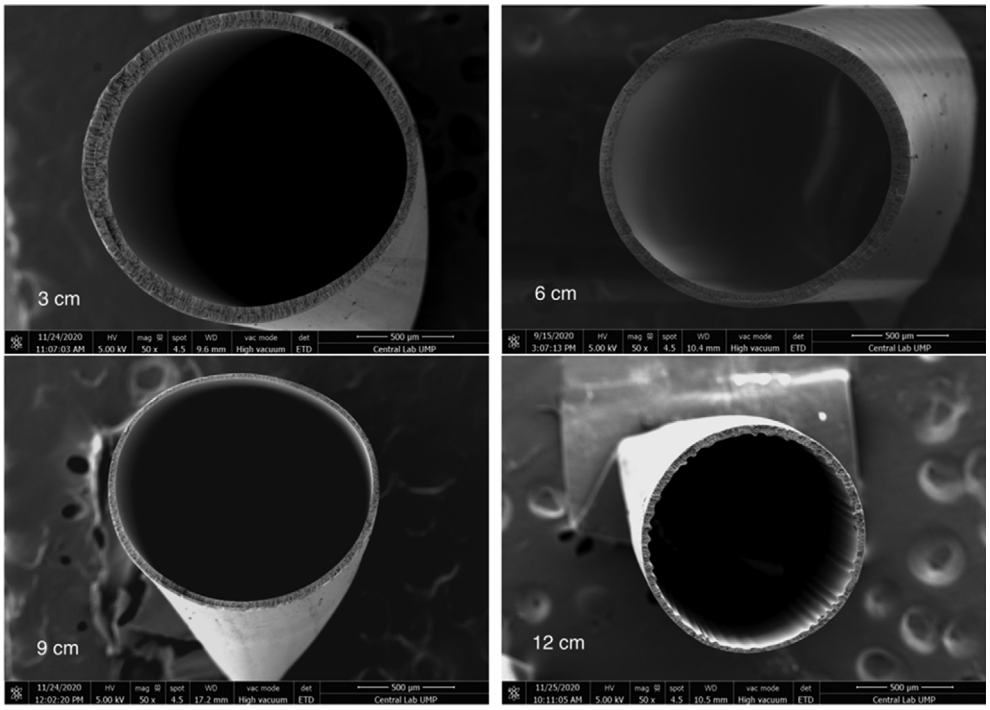

(a)

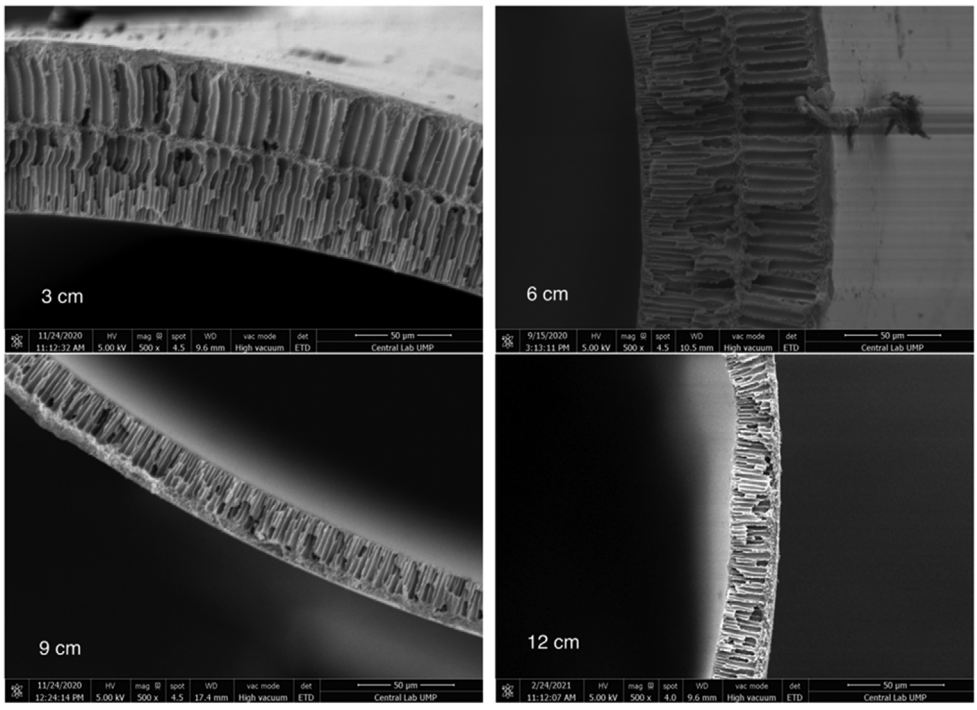

(b)

Fig. 7. Morphology of the HF membrane spun at different air gaps. (a) cross section, (b) thin wall section, (c) thick wall section.

est air gap of 3 cm. Korminouri et al. [11] found a similar pattern, stating that increasing the air gap from 1 to 20 cm enhanced the hydrophobicity of the PVDF membrane surface. The increase in the air gap from 3 cm to 12 cm increased the exposure time of the spinneret dope to the humidified environment. The moisture content in the environment instigated the vapor-induced phase inversion in the outermost layer of the dope before it entered the coagulation bath. This increased the formation of pores on the fiber surface, as shown in Fig. 7. As a result, the porous surface enhanced the hydrophobicity property of the fiber [31,33]. The exchange of

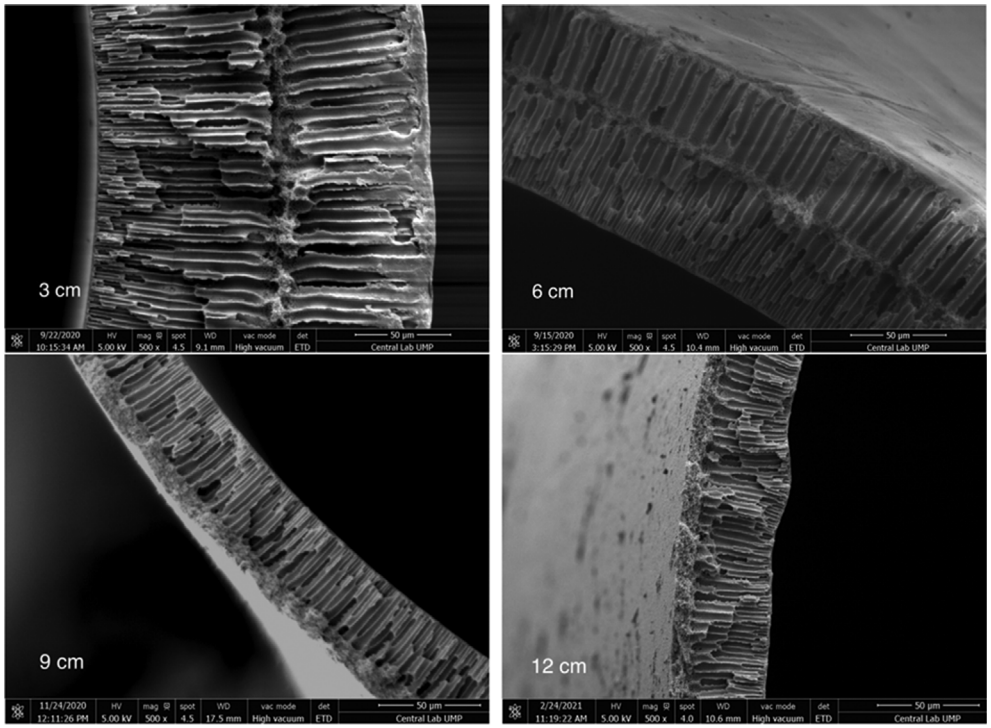

(c)

Fig. 7. Continued.

Table 3. Physical properties of the HF spun at different air gaps

Air Gap (cm)	3	6	9	12
ID (mm)	1.4560	1.3952	1.2160	1.0820
OD (mm)	1.6760	1.5574	1.3360	1.1820
Wall thickness (mm)	0.1100	0.0811	0.0600	0.0500
Total fiber volume (cm^3)	0.1624	0.1128	0.0722	0.0533
Empty space (cm^3)	0.1275	0.0875	0.0481	0.0306
Porosity (%)	78.5±3.06	77.57±2.77	66.70±1.50	57.40±2.03

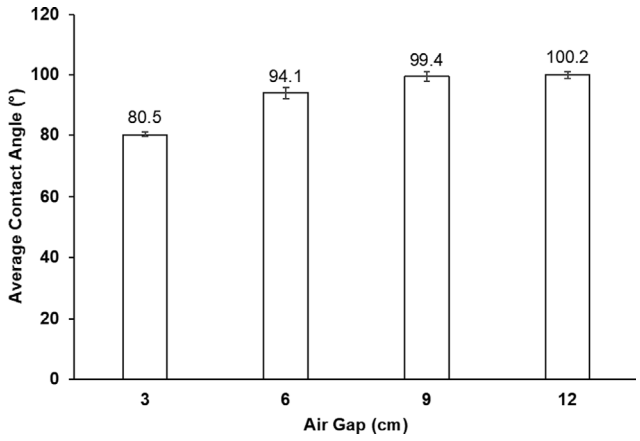

Fig. 8. Contact angle readings of fibers spun at different air gaps.

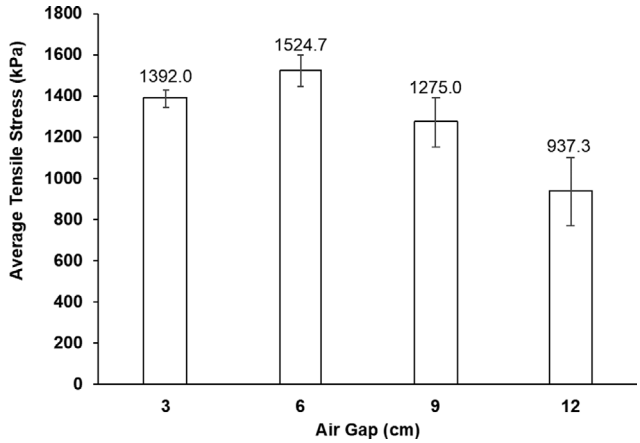

Fig. 9. Tensile stress readings of fibers spun at different air gaps.

solvent and moisture had not occurred at the short exposure time. The nascent fiber directly entered the coagulation bath and formed a dense skin layer at the innermost and outermost surface of the fiber [12]. Therefore, the fiber made from a 3 cm gap resulted in a

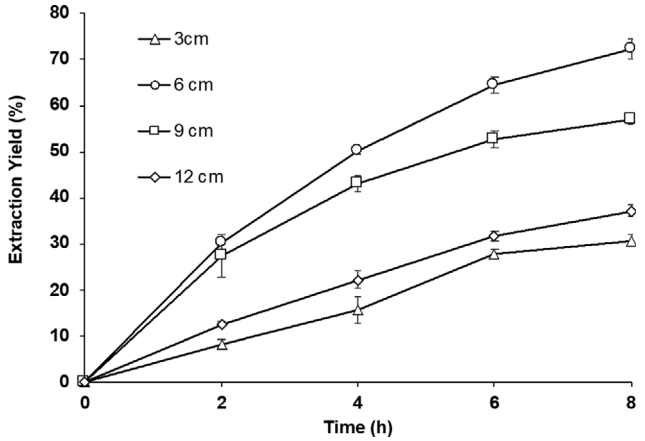

Fig. 10. Extraction yield of LA using HF spun at different air gaps. Experimental condition: feed phase - 10 g/L LA; stripping phase - 0.5 M NaOH; flow rate - 1 mL/min); LM phase - 0.3 M TOA in 2-ethyl-1-hexanol.

hydrophilic surface with the lowest contact angle reading of 80.5°.

According to Fig. 9, the tensile stress of the fiber increased from an air gap of 3 cm to 6 cm from 1,392.0 kPa and 1,524.7 kPa, respectively. A porous or open layer support was formed at an air gap of 6 cm. This open support layer improved the mechanical strength of the fiber [34]. Thus, it can remain stable in the SLM system without any breakage for an extended period of time. Further increases in the air gap above 6 cm drastically reduced the thickness and tensile stress of the fiber. Hence, the thin fiber spinneret at an air gap of 9 cm and 12 cm easily breaks under tension. Even though the 12 cm air gap may induce the highest open support surface, the asymmetric thickness with a very compact structure at the outer surface and a very porous or loose structure at the inner surface resulted in the lowest tensile stress, 937.3 kPa.

Fig. 10 shows the LA extraction using HF fabricated at different air gaps in HFLSM. The lowest LA extraction (30.7%) was demonstrated by the HF prepared at a 3 cm air gap distance. The skin layer formed at the inner and outer surface of the fiber spun at a 3 cm air gap had interrupted the interaction between the organic and stripping phases. Furthermore, the thick fiber accumulated more organic LM phase and resulted in the highest accumulation of the acid-amine complex in the organic phase. Consequently, it slowed the transport mechanism of the complexes and resulted in the lowest extraction of the LA. Although the fibers spun at 9 cm and the 12 cm air gap only had a dense outer layer, its porous outermost layer led to interaction between the organic and stripping phases. Thus, improving the LA extraction yield for HF spun at 9 cm and 12 cm was 57.1% and 37.2%, respectively. However, the thinnest fiber from 12 cm had the shortest LA diffusion pathway and easily induced a water bridge formation in LM [23]. Thus, it directly caused leakage of the liquid membrane to the stripping phase.

The highest LA extraction of 72.2% was achieved by the fiber spun at a 6 cm air gap. It had porous inner and outer surfaces with a medium wall thickness of 0.0811 mm. This structure provided good interaction between the LM phases, reduced the accumulation of LA or complexes, and enhanced the transportation of LA from the feed to the stripping phase. Therefore, an open porous surface membrane with a high LA extraction of 72.2% that was created via a 6 cm air gap was chosen for further HF spinning

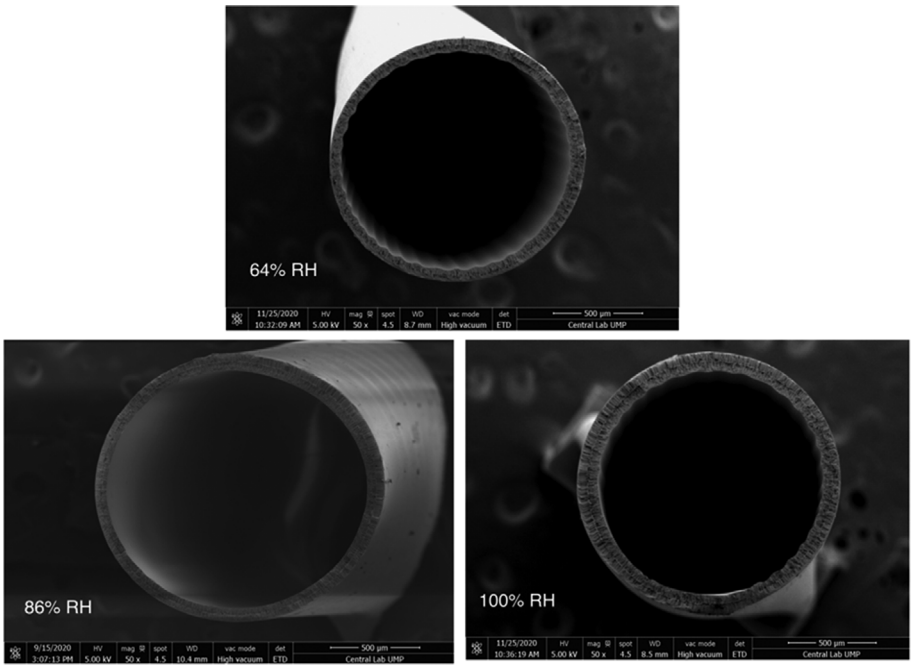

(a)

Fig. 11. Morphology of the HF membrane spun at different relative humidity: (a) cross section, (b) thin wall section, (c) thick wall section.

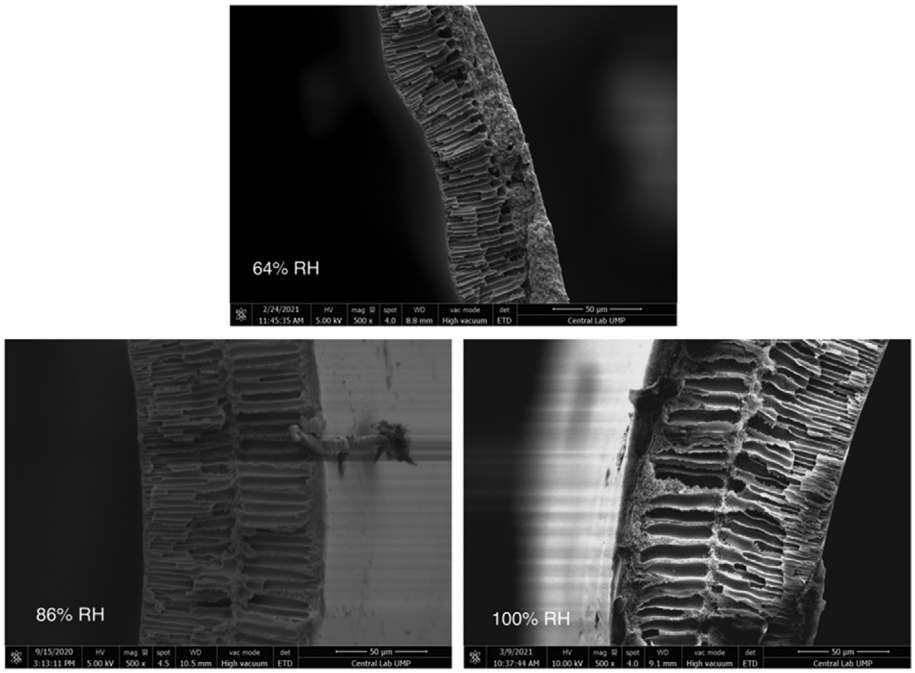

(b)

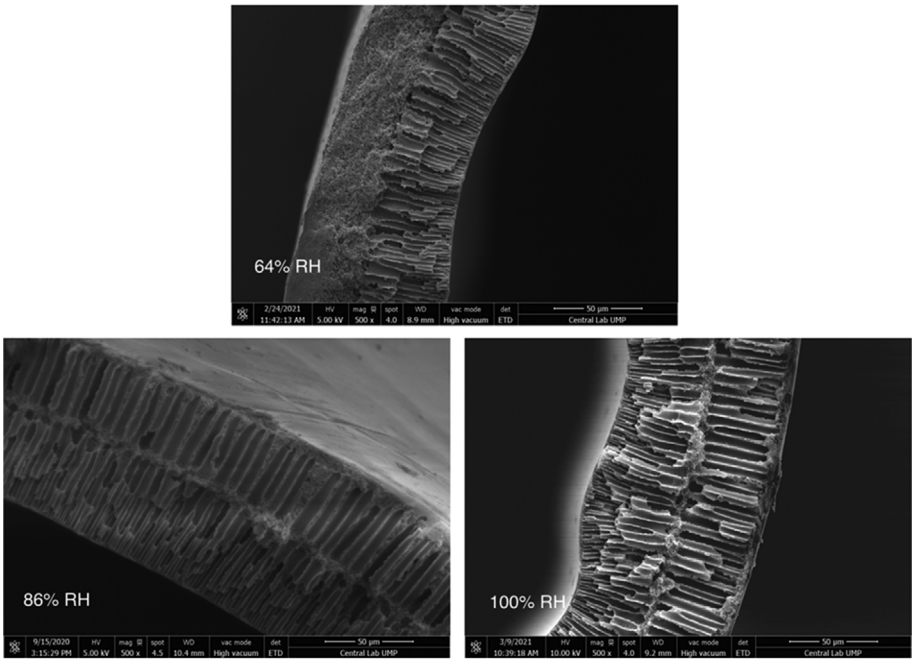

(c)

Fig. 11. Continued.

investigation.

3. Effect of Relative Humidity

Fig. 11 shows the morphology of the HF membrane prepared at different relative humidity. Table 4 shows the physical properties of the HF produced. At low air relative humidity (64%), the solvent within the thin film diffused more easily and rapidly from the cast film than the water vapor diffusion into the film, thus forming a denser layer at the outmost layer of fiber [35,36]. The dense layer formed at this low relative humidity (64%) resulted in the lowest outer and inner diameters of 1.4089 mm and 1.2680 mm, respectively. The increase in the relative humidity eliminated the formation of a dense outermost layer by forming a dual finger-like structure, as shown by the membrane prepared at 86% and 100% air relative humidity.

The fiber with the largest OD and ID diameters of 1.5574 mm and 1.3952 mm was formed at 86% air humidity. However, at 100%

Table 4. Physical properties of the fibers spun at a different relative humidity

Relative humidity (%)	64	86	100
ID (mm)	1.2680	1.3952	1.2900
OD (mm)	1.4089	1.5574	1.4950
Wall thickness (mm)	0.0705	0.0811	0.1025
Total fiber volume (cm^3)	0.0889	0.1128	0.1345
Empty space (cm^3)	0.0794	0.0875	0.1250
Porosity (%)	89.32±1.22	77.57±2.77	92.96±1.50

humidity, the film failed to absorb the water vapor completely and induced partial water condensation on the cast film surface [36]. Hence, it formed a thin and dense layer at the outer fiber and slightly reduced the diameter of the OD and ID by 4% and 7.5%, respectively, compared to HF at 86% air humidity. The outer layer of the fiber shrank at 64% air humidity to produce a compact and dense skin layer. It produced the thinnest HF with a wall thickness of 0.0705 mm. The increase in the humidity to 86% and 100% enhanced the water vapor uptake in the cast film and improved the growth of pores. Consequently, the mean pore diameter enlarged and improved the thickness of the fibers [36]. It also led to a high amount of empty space in the fibers, as shown in Table 4.

An increase in the air humidity increased the pore formation and empty space from 0.0794 cm^3 to 0.1250 cm^3. The massive number of large pores in the fiber spun at 100% gave rise to the highest porosity value of 92.96%. The reduction in air humidity reduced the sizes and formation of macrovoids, thus reducing the porosity to 77.57%. Generally, a porosity of 70% and above is suitable to be in the SLM process [6,37,38]. The formation of a large number of interconnected micropores at the dense layer and the formation of a single finger-like at the bottom layer enhanced the porosity of the fiber spun at room humidity to 89.32%.

Based on Fig. 12, the highest surface contact angle reading was achieved at low humidity. It might be due to the accumulation of graphene at the top surface. At 86% air humidity, the contact angle reading dropped to 94.1°. Theoretically, the membrane support is classified as hydrophobic and superhydrophobic when the membrane contact angle is greater than 90° and greater than 150°, respectively [39]. Hence, the fiber spun at 86% relative humidity represents a hydrophobic property. The smooth and dense layer formation due to the water condensation effect at high humidity of 100% reduced the contact angle reading to 79.6° and showed a hydrophilic property.

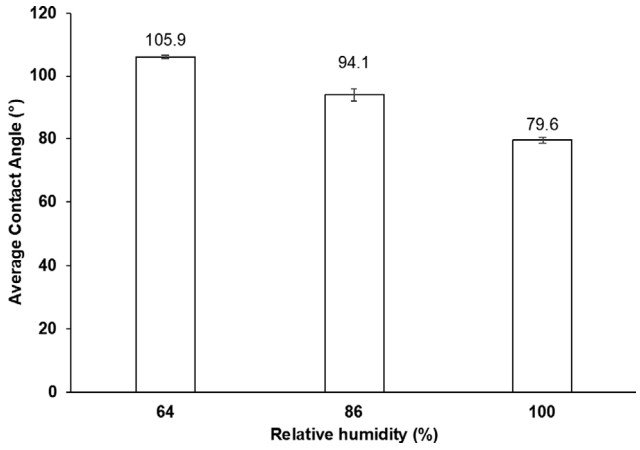

Fig. 12. Contact angle readings of fibers spun at different relative humidity.

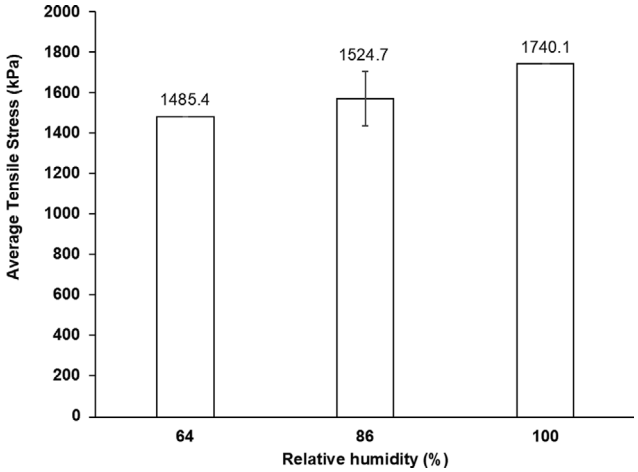

Fig. 13. Tensile stress readings of fibers spun at a different relative humidity.

According to Fig. 13, the fiber with a dual finger-like structure possesses high mechanical strength and can withstand high pressure without a break. The highest tensile stress of 1,740.1 kPa is achieved by the porous and the thickest fiber spun at high humidity of 100%. Hence, their chains are not easily reoriented to the flow rate or pressure changes. However, the unsymmetric fiber was easily broken under a low pressure of 1,485.4 kPa.

The extraction yield of LA using fibers spun at different relative humidity is shown in Fig. 14. At an optimum air humidity of 86%, the fiber open pore structure and the largest internal and external surface areas of 13.1495 cm^2 and 14.6778 cm^2, respectively, enhancing the interaction between the SLM phase and the LA transport. Furthermore, its porous structure had a high possibility of induc-

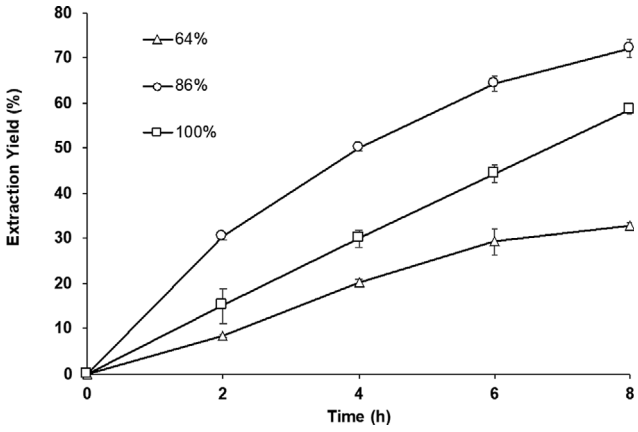

Fig. 14. Extraction yield of LA using fibers spun at different relative humidity. Experimental condition: feed phase - 10 g/L LA; stripping phase - 0.5 M NaOH; flow rate - 1 mL/min); LM phase - 0.3 M TOA in 2-ethyl-1-hexanol.

ing an efficient convective flow in the SLM system [40]. Consequently, the highest LA extraction of 72.2% was achieved. However, the dense layer in fiber at 64% air humidity acts as a barrier between the organic and stripping phase. Moreover, diffusion is the only way for mass transport through a dense fiber layer [40]. Diffusion only carries a small amount of LA-TOA complex to the membrane interface and restricts the stripping of the LA to the stripping. It indirectly limits the extraction of LA to 32.8%. Besides the dense layer, the thick wall and huge amount of LM in fiber spun from 100% gave rise to the accumulation of the LA-TOA complex. Thus, it slows the transport mechanism of the complex and lowers the extraction yield to 58.7% [41].

CONCLUSION

Based on the study, the properties and morphology of the PES membrane can be easily modified by controlling the spinning parameters. The fiber properties and morphology highly impact its performance in SLM for LA extraction. Among the factors, the bore liquid is the most significant that greatly impacts the LA extraction. The skin layer formation was successfully reduced by reducing the concentration difference between the bore liquid and the spun dope solution. The porous outer surface fiber can be adjusted by varying the air gap distance and relative humidity of the spinning environment. Using bore liquid composed of 60% v/v DMAC in water at air gap and relative humidity of 6 cm and 86%, respectively, an effective membrane support with optimal membrane thickness and an open porous surface for a high LA extraction was produced. The highest LA extraction of 72.2% was accomplished using the optimized membrane support in HFSLM.

ACKNOWLEDGEMENT

Vikneswary Rajendaren would like to express her gratitude to the Universiti Malaysia Pahang for sponsoring her Ph.D. study under the UMP Doctoral Research Scheme (DRS).

FUNDING

This work was supported by the Ministry of Higher Education, Malaysia through Fundamental Research Grant Scheme [RDU170117 - FRGS/1/2017/TK02/UMP/02/8].

CREDIT AUTHOR STATEMENT

Vikneswary Rajendaren: Investigation, Writing - Original Draft; **Syed M. Saufi**: Supervision, Conceptualization, Writing - Review & Editing; **M. A. K. M. Zahari:** Supervision, Conceptualization.

CONFLICT OF INTEREST

The authors declare that they have no conflicts of interest.

REFERENCES

1. V. G. Yadav, G. D. Yadav and S. C. Patankar, *Clean. Technol. Environ. Policy*, **22**, 1757 (2020).
2. X. Lin, Q. Huang, G. Qi, S. Shi, L. Xiong, C. Huang, X. Chen, H. Li and X. Chen, *Sep. Purif. Technol.*, **174**, 222 (2017).
3. A. E. Tugtas, *Fen Bilimleri Dergisi*, **23**, 70 (2011).
4. V. Rajendaren, S. M. S. M. Saufi, M. A. K. A. K. Zahari, A. W. Mohammad and A. Wahab, *Mater. Today Proc.*, **17**, 1117 (2019).
5. V. Rajendaren, S. M. Saufi, M. A. K. M. Zahari, N. Othman and R. N. R. Sulaiman, *Korean J. Chem. Eng.*, **38**, 2519 (2021).
6. A. Didi and M. A. Didi, *Sci. Study Res.*, **X2**, 149 (2009).
7. V. S. Kislik, Liquid Membranes, Principles and Applications in Chemical Separations & Wastewater Treatment (2009).
8. T. Wongsawa, N. Leepipatpiboon, N. Thamphiphit and U. Pancharoen, *Chem. Eng. J.*, **222**, 361 (2013).
9. Y. Liu, G. H. Koops, and H. Strathmann, *J. Membr. Sci.*, **223**, 187 (2003).
10. A. F. Ismail, M. I. Mustaffar, R. M. Illias and M. S. Abdullah, *Sep. Purif. Technol.*, **49**, 10 (2006).
11. F. Korminouri, M. Rahbari-Sisakht, D. Rana, T. Matsuura and A. F. Ismail, *Sep. Purif. Technol.*, **132**, 601 (2014).
12. N. Said, H. Hasbullah, A. Fauzi, M. Nidzhom, A. F. Ismail, M. Nidzhom, Z. Abidin, P. Sean and M. H. Dzarfan, *Chem. Eng. Trans.*, **56**, 1591 (2017).
13. A. L. Ahmad, Z. Mohamad and H. Mohd, *J. Phys. Sci.*, **28**, 185 (2017).
14. M. Khayet, *Chem. Eng. Sci.*, **58**, 3091 (2003).
15. N. Ismail, A. Venault, J. Mikkola, D. Bouyer, E. Drioli and N. T. H. Kiadeh, *J. Membr. Sci.*, **597**, 117601 (2020).
16. Y. Gencal, E. N. Durmaz and P. Z. Culfaz-emecen, *J. Membr. Sci.*, **476**, 224 (2015).
17. F. A. AlMarzooqi, M. Roil Bilad and H. Ali Arafat, *Appl. Sci.*, **7**, 181 (2017).
18. N. Harruddin, S. M. Saufi, C. K. M. Faizal and A. W. Mohammad, *RSC Adv.*, **8**, 25396 (2018).
19. S. Sanmugam, N. Harruddin and S. M. Saufi, *Chem. Eng. Res. Bull.*, **19**, 118 (2017).
20. Q. F. Alsalhy, H. A. Salih, S. Simone, M. Zablouk, E. Drioli and A. Figoli, *Desalination*, **345**, 21 (2014).
21. Y. Manawi, V. Kochkodan, E. Mahmoudi, D. J. Johnson, A. W. Mohammad and M. A. Atieh, *Sci. Rep.*, **7**, 1 (2017).
22. D. Li, R. Wang and T.-S. Chung, *Sep. Purif. Technol.*, **40**, 15 (2004).
23. A. J. B. Kemperman, D. Bargeman, Th. van den Boomgaard and H. Strathmann, *Sep. Sci. Technol.*, **31**, 2733 (1996).
24. A. Kumar and A. M. Sastre, *Ind. Eng. Chem. Res.*, **39**, 146 (2000).
25. N. S. Rathore, J. v. Sonawane, A. Kumar, A. K. Venugopalan, R. K. Singh, D. D. Bajpai and J. P. Shukla, *J. Membr. Sci.*, **189**, 119 (2001).
26. R. Güell, E. Antic, V. Salvad and C. Fontàs, *Sep. Purif. Technol.*, **62**, 389 (2008).
27. T. Pirom, N. Sunsandee, P. Ramakul, U. Pancharoen, K. Nootong and N. Leepipatpiboon, *J. Ind. Eng. Chem.*, **23**, 109 (2015).
28. A. Idris, N. Mat Zain and M. Y. Noordin, *Desalination*, **207**, 324 (2007).
29. Y. Bang, M. Obaid, M. Jang, J. Lee, J. Lim and I. S. Kim, *Chemosphere*, **259**, 127467 (2020).
30. C. Cao, T. S. Chung, S. B. Chen and Z. J. Dong, *Chem. Eng. Sci.*, **59**, 1053 (2004).

31. K. Y. Wang, D. F. Li, T. S. Chung and S. B. Chen, *Chem. Eng. Sci.*, **59**, 4657 (2004).
32. T. H. Young and L. W. Chen, *Desalination*, **103**, 233 (1995).
33. D. Y. Guo, C. H. Li, L. M. Chang, H. C. Jau, W. C. Lo, W. C. Lin, C. T. Wang and T. H. Lin, *Polymers* (Basel), **12**, 1 (2020).
34. R. W. Baker, *Membrane technology and applications*, John Wiley & Sons, Ltd, Chichester, UK (2004).
35. E. Fontananova, V. Cucunato, E. Curcio, F. Trotta, M. Biasizzo and G. Barbieri, *Electrochim. Acta*, **66**, 164 (2012).
36. C. Meringolo, T. F. Mastropietro, T. Poerio, E. Fontananova, G. de Filpo, E. Curcio and G. di Profio, *ACS Sustain. Chem. Eng.*, **6**, 10069 (2018).
37. C. Fontas, R. Tayeb, S. Tingry, M. Hidalgo and P. Seta, *J. Membr. Sci.*, **263**, 96 (2005).
38. A. Ito, *J. Membr. Sci.*, **175**, 35 (2000).
39. N. A. Ahmad, C. P. Leo, A. L. Ahmad and W. K. W. Ramli, *Sep. Purif. Rev.*, **44**, 109 (2015).
40. E. Nagy, in *Basic equations of mass transport through a membrane layer*, edited by K. Marinakis, 2nd ed., Susan Dennis, Hungary, 185 (2019).
41. N. Harruddin, S. M. Saufi, C. K. M. Faizal and A. W. Mohammad, *Chem. Eng. Trans.*, **56**, 847 (2017).